Wavefront Preservation in Soft X-Ray Beamlines for the Advanced Light Source Upgrade

ANTOINE WOJDYLA AND KENNETH A. GOLDBERG, ON BEHALF OF THE ALS-U BEAMLINE AND OPTICAL SYSTEMS TEAM

Advanced Light Source, Lawrence Berkeley National Laboratory, Berkeley, California, USA

Introduction

In the 4th generation of X-ray light sources, including Free-Electron Lasers (FEL) and Diffraction-Limited Storage Rings (DLSR), the emittance of the electron beam is small or negligible compared to the emittance of the photon beam produced by insertion devices, thus generating coherent beams of light. Over the next few years, several light-source facilities will be built or upgraded to produce X-ray beams of unprecedented coherent flux. Delivering these exceptional beams to the sample chambers requires beamline optical systems that are designed to preserve the wavefront properties. Our goal in the Advanced Light Source upgrade project (ALS-U) is to create a new class of beamlines that reach diffraction-limited X-ray optical quality through tightly integrated, efficient optical systems, diagnostics, and adaptive mirrors, thus providing users with new scientific capabilities offered by coherent X-ray light interactions with matter. Here we describe aspects of the beamlines' design as they enter the project's final design phase.

Insertion device beamlines for the upgraded ALS

The upgrade of the Advanced Light Source (ALS-U) entails three key aspects [1]. An accumulator ring enables on-axis, swap-out injection for continuous high electron-beam current; a new, 9-bend, multi-bend achromat (MBA), 2 GeV storage-ring lattice creates a symmetric low-emittance beam; and a set of four new and upgraded insertion-device beamlines preserve the beam properties from the source to the sample. The new storage ring will reduce the horizontal beam size from 250 μm-rms to 12 μm-rms and produce a round, diffraction-limited soft X-ray photon beam with two orders of magnitude higher coherent flux than the existing ALS.

While the new and upgraded beamlines have various scientific goals, they are being designed together, sharing many elements of a common design framework. They are driven by linear or elliptically polarizing undulator (EPU) sources. Most will offer a modest photon-energy resolution (5,000 resolving power) and moderate demagnification (typically 5×) for imaging and scattering scientific programs covering the soft X-ray regime: *MAESTRO-U* (60–600 eV), *FLEXON* (230–1,400 eV), *COSMIC-U* (250–2,500), and *Tender* (1000–8,000 eV).

The beamlines have been designed, modeled, and optimized using a variety of available tools, including OASYS [2] based on SHADOW [3], Sirepo [4] based on SRW [5], and SPECTRA [6]. Their efficient optical designs are based on two vertical and two horizontal reflective elements (Figure 1). The flat, white beam mirrors deflect the beam horizontally, filtering unwanted high-energy light, and providing an opportunity for diversion into multiple branches on two of the beamlines. These mirrors will be made from cryogenically cooled silicon substrates to minimize thermal distortion from the intense and dynamically varying X-ray beam [7]. The grating monochromator is based on a variable

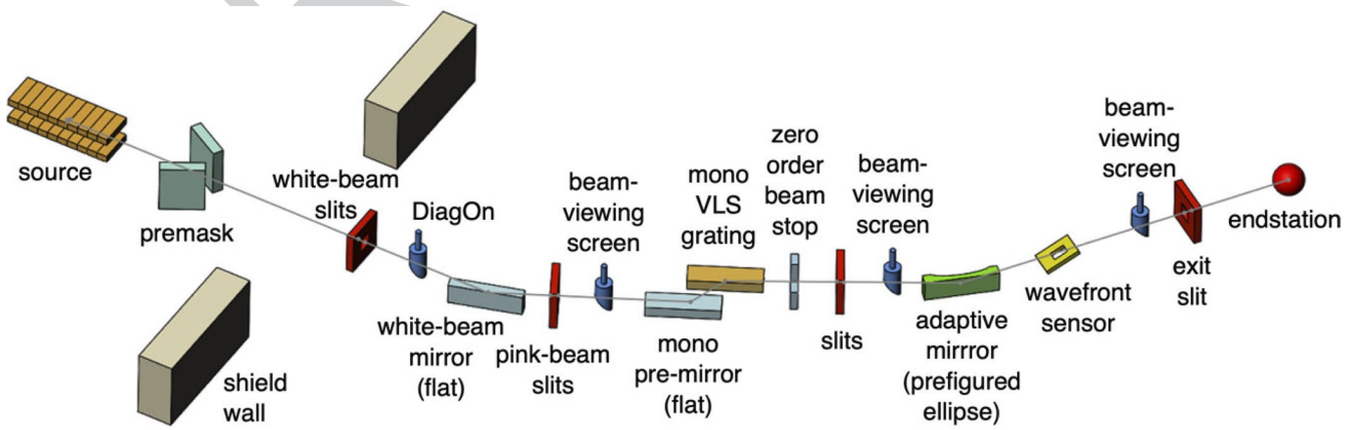

Figure 1: Optical layout of a typical ALS-U beamlines (COSMIC upgrade).

included angle, variable line spacing grating (VIA-VLS) design [8], and provides both photon energy dispersion and vertical focusing to the exit-slit plane. The final, horizontal focusing mirror is a piezo-bimorph deformable mirror, pre-figured to the optimal elliptical shape at rest. It is paired with an intermittently insertable wavefront sensor placed directly downstream to measure the cumulative upstream wavefront aberrations in the beam, for correction with the adaptive shape control. A suite of beam-positioning diagnostics is integrated into the design to measure slow drifts and rapid vibration. On each branch, a horizontal beam-position diagnostic integrated into the exit slit provides feedback for active beam stabilization up to about 100 Hz, using the tilt angle of the adaptive mirror.

Tolerancing beamline optical systems for coherent X-ray light

Our approach to the specification and tolerancing of beamline optics begins with the recognition that coherent light requires careful attention be paid to the wavefront, in addition to the slope errors and curvature radii. Our goal is to maintain a Strehl ratio above 0.8 (the Maréchal criterion, related to the beam intensity at focus [9]), putting stringent demands on the inherent optical surface shapes, their mutual alignment, the presence of surface contamination, and even the ruling of monochromator gratings. Wavefront errors can accrue from each of these sources. We view the adaptive corrections as a means to perfect a beam that is already high quality, so the beamline elements are designed to meet our specifications in their ground state.

Regarding the wavefront, our mirror specifications are derived from a surface height error metric that is calculated with a beam amplitude weighting that matches the physical diffraction equation [10]. This metric is closely tied to the Strehl ratio at the beamline focus. We aim for weighted-rms wavefront error below $\lambda/14$ across the operating range. We note that as the wavelength is reduced with photon energy, the beam footprint also shrinks. For errors of the low-spatial frequencies, it is perhaps counterintuitive that satisfying the surface requirements at the lowest photon energy satisfies the requirements across the entire range. Typically, cumulative rms height errors are limited to approximately 5 nm, with a smaller error budget apportioned to each element.

Slope error considerations arise from the finite source size and the optical distances in the beamline. A 2-m-long undulator at 1 keV photon energy has an effective source size of $\sigma = 20$ µm and beam divergence of $\sigma' = 20$ µrad. To maintain the focused beam quality, we set the slope error tolerances to constrain the beam broadening to 5% of the effective beam width at focus, based on geometric magnification. Slope error tolerances for our beamline mirrors are as tight as 50 nrad rms, but are more typically 150 nrad.

Allowable errors in the radii of curvature of the first, flat mirror depend on the apparent longitudinal size of the source, or *source depth,* z_d (this is $z_d = \sigma/\sigma' \approx 1$ m in our case). The tolerable radius of curvature is below ROC< $(p^2/z_d)\cdot(2/\sin\theta)$, typically 20 km for ALS-U. This is stricter than the 2 km tolerance for the current ALS, with its much larger horizontal source size (250 µm-rms vs. 20 µm-rms), owing to the gains from reduced electron-beam emittance.

Cryogenically cooled white-beam mirrors

Insertion devices in the upgraded ALS will produce high X-ray power densities at the first beamline mirror (up to 200 W/mm^2) that vary on relatively short time scales during routine operation. Since nanometer-scale surface deformations can critically impact the wavefront quality, the mitigation of thermal distortion poses a significant challenge, especially for the leading, white-beam mirror in the beamline. The problem is acute on EPU beamlines where changes in the insertion-device deflection parameter and the rotation of the polarization vector stretch or compact the beam footprint within seconds.

When designing beamlines to maintain performance across a broad range of operating conditions, we focus on the most challenging cases: these are the highest K values, with peak incident power up to 200 W, and where the beamline aperture (frontend slits) is the largest. For each mirror, SPECTRA was used to generate the spatial distribution as a function of photon energy. The absorbed power was calculated from the energy-dependent reflectivity of each coating (more recently, this important capability has been ported from SRCalc into OASYS as the *IDPower* widget [11]). We then feed the absorbed power profiles into the finite-element method software ANSYS to predict the height deformation of the mirror surface as a function of the mirror geometry and cooling strategy. Our rms weighted height error metric is used to qualify the designs in the extreme cases. Although each beamline is unique, we developed a standard white-beam mirror design suitable for all four beamlines.

We initially meant to design a water-cooled horizontally deflecting white beam mirror, and we ran a large quantity of simulations for various materials, geometries of water-cooling channels and additional notches (Figure 2a), strategies known to work for near-constant heat-load conditions [12]. The result of these simulations is summarized in Figure 2, where the resulting weighted height errors for two polarization conditions are plotted against each other. No single water-cooling geometry could be identified that satisfied our requirements in all cases (Figure 2b).

Within the project, all white-beam mirrors will be cryogenically cooled to exploit the special, low-temperature properties of silicon: the thermal expansion coefficient crosses zero near 125 K, allowing the mirror surface shapes to be much more resilient to varying power loads.

The cryo-cooled mirrors will be supported on one end, attached to a cooling block in a cantilevered geometry (Figure 3). Liquid nitrogen is the cooling medium. This approach avoids potential stresses from mismatched thermal expansion that could occur with mirrors and mounts cooled to 125 K from room temperature [7]. A prototype has been developed to validate the thermal modeling and to ensure that the flat mirror shape is preserved upon cooling [13].

Using the VLS monochromator to compensate vertical wavefront errors

The monochromator consists of two reflections: a flat pre-mirror and a VLS grating (Figure 4). Several different gratings (typically three) are ruled side-by-side on the substrate to efficiently span the op-

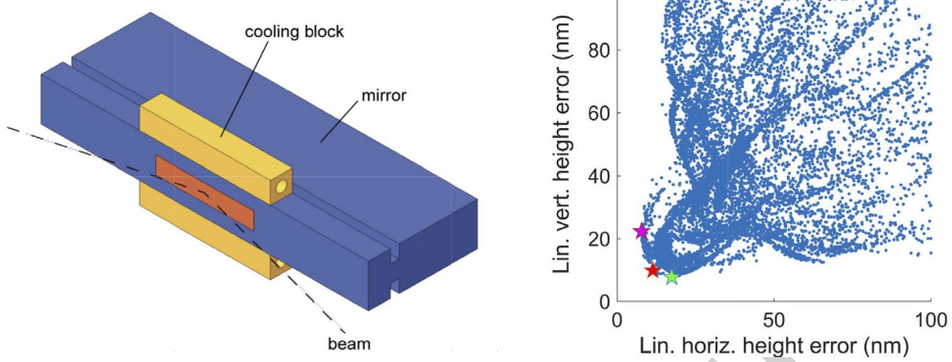

Figure 2: Initial white beam mirror design with water cooling: (a) mirror geometry and side-cooling; (b) figure of merit of candidate designs during the design optimization process.

erating energy range. The grating rotates about its central point of intersection, while the pre-mirror both rotates and translates to maintain an ideal angle of incidence and a stable beam position on the grating. Since the pre-mirror receives a variable high power load, there is concern that it will experience thermal deformation. Modeling suggests that this will be dominated by a second-order tangential bump, much broader than the central, monochromatic portion of the beam, causing a vertical defocus if left uncorrected.

To correct this error, we recognize that the VLS grating effectively operates as a 1D reflective zoneplate, where the focal distance varies with wavelength and angle of incidence. Using an approach first described by Reininger [14], defocus errors can be compensated by making a slight modification of the fixed focus constant (c_{ff}), determined by the relative angles between the pre-mirror and the monochromator (Figure 4a).

For a VLS gratings with a nearly linear variation in the line density, defined as $g(x) = g_0 + 2b_2g_0x + O(x^2)$, c_{ff} is almost constant along the monochromator trajectory. With p and q as the object and image distances, we find $c_{ff} \approx (b_2 + 1/p)/(b_2 - 1/q)$. A change in the wavefront radius of curvature R induces a displacement of the effective source distance: $p' = 1/(2/(R\sin\theta) - 1/p)$, and the new c_{ff} can be calculated accordingly (Figure 4b). Raytracing simulations show that radius of curvature errors in the pre-mirror down to 1 km can be compensated by adjusting the grating monochromator angles, without loss of photon energy resolution (Figure 4c) or a change in the focused beam spot size.

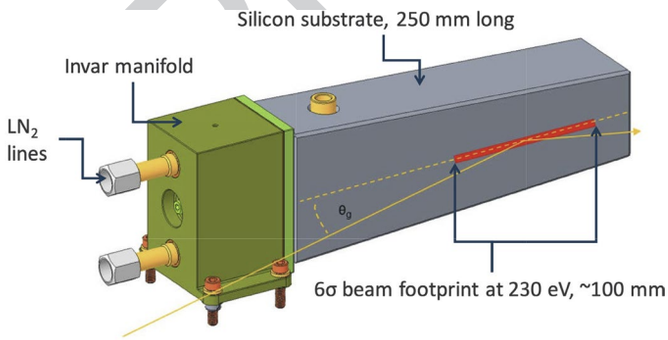

Figure 3: Cryo-cooled cantilevered white beam mirror design for ALS-U beamlines.

Compensating upstream aberrations using the X-ray adaptive mirror

The piezo-bimorph adaptive X-ray mirror is the final mirror in the beamline and the only horizontally focusing element. It will be prefigured into the ideal elliptical shape while at rest. Fine shape adjustments are controlled by more than 10 separate actuator channels along its length, allowing it to compensate small errors in the incident wavefront and restore a nearly ideal wavefront shape.

In 2019, with a commercially available adaptive mirror of similar design, we collected shape-control performance data using a beamline and X-ray wavefront sensor at the Advanced Photon Source [15]. The mirror is 160 mm long and 50 mm wide, with a thickness of 10 mm, and it has 18 actuator channels. Static influence functions were measured for each of the actuators (Figure 5a). The peak deformation sensitivity (at the center) is about 1 nm/V, over a 500 V range, capable of 1.5 µm total sag. We found that the residual error is typically a few percent of the total motion, suitable for most anticipated applications. We used the influence functions to build a linear model of the mirror in OASYS, and predict that the adaptive mirrors can compensate convex or concave errors in the white beam mirror with an error radius of curvature as small as 1 km (Figure 5b) [16].

Feedback from intermittent, reflective wavefront sensors

Feedback for the cumulative upstream beam focusing comes from wavefront sensors placed after the adaptive mirror. In this zone, upstream of the beamline focus, the beam is narrow (typically 1–3 mm wide) and converging, and it is vertically dispersed by the monochromator, smearing the wavefront vertically. Each individual branchline will be equipped with a one-dimensional wavefront sensor tailored for operation in these challenging conditions. They are designed for

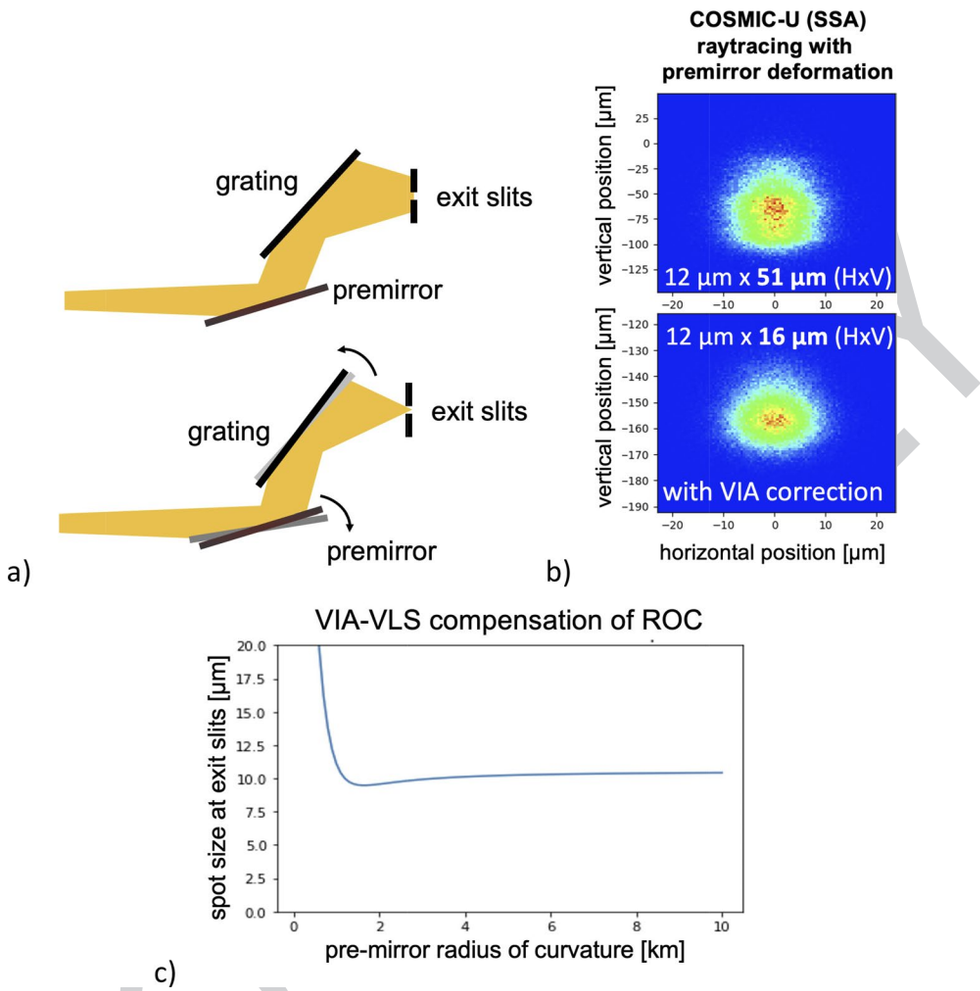

Figure 4: Variable line spacing grating for the compensation of heatload deformations on the pre-mirror: (a) adjusting the focal distance by changing trajectories; (b) example of a raytracing simulation (Shadow/OASYS) including pre-mirror deformation, and compensation by adapting the VIA-VLS trajectory; (c) achievable beam size at exit slits using VIA-VLS trajectory compensation for various pre-mirror radius of curvature.

minimally invasive operation with rapid, intermittent insertion and removal, providing direct feedback to drive the shape correction of the adaptive mirror that immediately precedes it.

We have developed and prototyped a novel soft X-ray wavefront sensor design based on a patterned, reflective grating array [17, 18] that operates at glancing incidence. Patterns for shearing interferometry and Hartmann wavefront sensing are deeply etched into a superpolished silicon-wafer chip. The etched grating structure forms a binary amplitude grating, blocking the reflection of unwanted light, and enabling high fringe contrast to be achieved. In the pattern, a compact array of individual gratings spans the operating energy range with each grating covering a dedicated portion. The chip is mounted to a mechanical flipper (Figure 6a) for rapid, stable insertion and removal from the beam path. Figure 6b shows a photograph of the prototype installed on an ALS beamline for testing in May of 2021.

Integrated beam diagnostics

While diagnostics are an afterthought in many beamline designs, our beamline designs integrated beam position monitors, fiducialized drop-in viewing screens, and other diagnostics at strategic locations from the earliest stages of development. Achieving and maintaining optimal beamline performance will require close attention to fine alignment over time.

In the highest power-density regions of the beamline, DiagOn-type beam position monitors [19] will be used to assess the beam alignment and to center the front-end apertures on the beam. These invasive monitors collect a relatively large solid angle of the beam, and use a narrowband reflection from a multilayer-coated mirror or crystal to select a specific photon energy for measurement. The observed pattern of rings and lobes depends sensitively on the insertion-device's deflection parameter, K, and on the beam polarization.

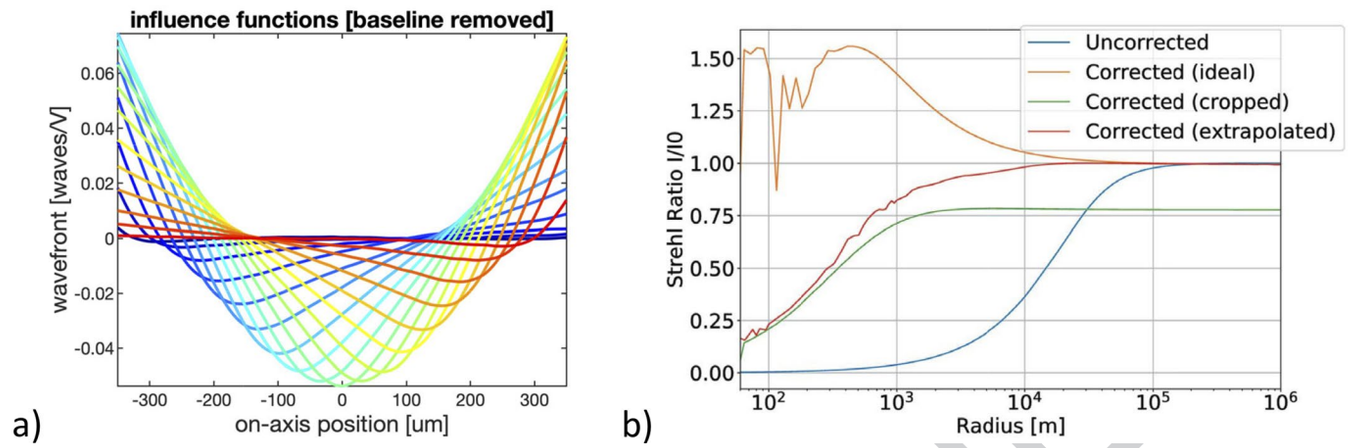

Figure 5: Deformable mirror and compensation of aberrations: (a) influence function from an X-ray deformable mirror measured at APS; (b) range of correctable radius of curvature from the white beam mirror in typical ALS-U cases.

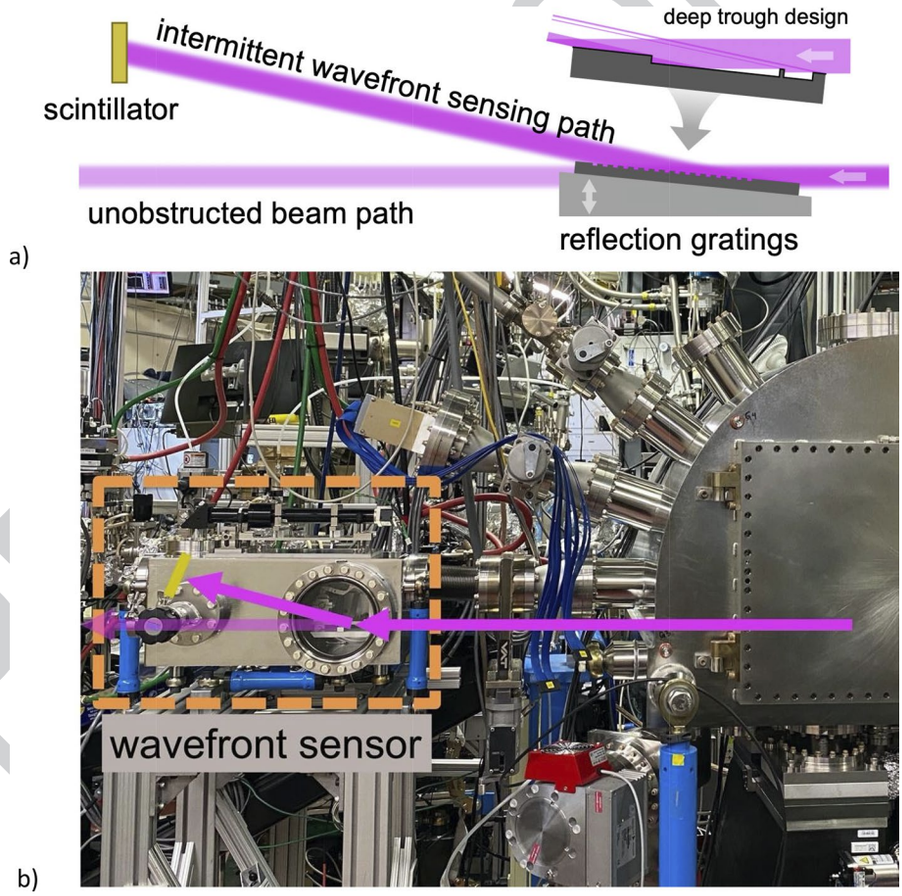

Figure 6: ALS-U wavefront sensor: (a) reflective grating and actuation for intermittent wavefront sensing; (b) the prototype installed on an ALS beamline.

The upstream side of most other mirrors will have a closely placed, insertable scintillator viewing screen equipped with an external, low-magnification microscope for position feedback. These diagnostics will allow us to observe the beam as it propagates and use tools currently being developed to optimize the alignment based on physical models [20].

In our designs, the aperture at each beamline focus will not be significantly overfilled, since in diffraction-limited beamlines the slit or pinhole at the secondary focus essentially serves as a mere spatial filter. However, horizontal beam motion can induce intensity fluctuation in the endstation. For this reason, photocurrent from the blades of the horizontal slit will be monitored for use as fast angular feedback at the adaptive mirror. Pitch actuation on the order of 100 Hz will be driven by mirror tilts on the order of tens of nanoradians. The vertical exit slits, which serve as photon energy selection on the vertically dispersed beam, will feature a polished reflective surface near the slit edge in order to divert part of the unused beam to reference elemental edges and a photodiode. This approach will provide real-time absolute photon energy feedback for the monochromator and for experiments that are sensitive to small energy fluctuations.

Keeping the systems clean

For extreme ultraviolet and soft X-ray beamlines especially, preventing the buildup of carbon contamination on optical surfaces is essential for intensity and wavefront preservation. Furthermore, particulate contamination can be highly detrimental to coherent beams and must be controlled. We have adopted strict UHV clean practices for materials specification, assembly, testing, and for long-term mirror storage prior to installation. For the mirrors with oxygen-compatible coatings, chambers will be outfitted with a low-partial-pressure oxygen bleed to prevent beam-induced carbon buildup over time. Furthermore, many of our optical assemblies will include an oxygen plasma generator to allow for in-situ cleaning of the optics where appropriate.

Conclusion

Extracting the highest possible performance from the new generation of coherent X-ray light sources requires efficient beamlines optical systems designed for diffraction-limited quality. The new and upgraded insertion device beamlines in the ALS-U project are built on simple yet robust optical designs with only four optical elements, and all are designed around a common framework. These beamlines will advance new technologies with cryogenically cooled white-beam mirrors, adaptive optics, and novel wavefront sensors, all tightly integrated with photon diagnostics for stable, resilient, optimized experimental systems. The beamlines will be able to diagnose and compensate a range of mild optical aberrations, restoring performance that would otherwise be lost. With commissioning a few years away, the promise of new scientific capabilities and discoveries enabled by high-power coherent X-ray light awaits. ■

References

1. A. White *et al.*, *Synchrotron Radiation News* **32** (1), 32 (2019). doi:10.1080/08940886.2019.1559608
2. L. Rebuffi *et al.*, *Proc. SPIE* **10388**, 103880S-1 (2017). doi:10.1117/12.2274263
3. M. Sanchez Del Rio *et al.*, *J. Synchrotron Rad.* **18** (5), 708 (2011). doi:10.1107/S0909049511026306
4. M. Rakitin *et al.*, *J. Synchrotron Rad.* **25** (6), 1877 (2018). doi:10.1107/S1600577518010986
5. O. Chubar *et al.*, *Proc. SPIE* **4769**, 145 (2002). doi:10.1117/12.481182
6. T. Tanaka, *J. Synchrotron Rad.* **28** (4), 1267 (2021). doi:10.1107/S1600577521004100
7. G. Cutler *et al.*, *J. Synchrotron Rad.* **27** (5), 1131 (2020)., doi:10.1107/S1600577520008930
8. K. Amemiya *et al.*, *J. Synchrotron Rad.* **11** (2), 171 (2004). doi:10.1107/S0909049503023598
9. X. Shi *et al.*, *Proc. SPIE* **9687**, 968703 (2016). doi:10.1117/12.2241139
10. K. Goldberg*et al.*, *Rev. Sci. Instrum.* **87** (5), 051805 (2016). doi:10.1063/1.4950747
11. L. Rebuffi *et al.*, *J. Synchrotron Rad.* **27** (5), 1108 (2020)., doi:10.1107/S160057752000778X
12. J. Knopp *et al.*, Proceedings of the MEDSI 2018 Conference, 2018, p. 238. doi:10.18429/JACoW-MEDSI2018-WEPH16
13. G. Cutler *et al.*, *Proc. SPIE* **11491**, 114910F (2020). doi:10.1117/12.2568101
14. R. Reininger *et al.*, *Rev. Sci. Instrum.* **79** (3), 033108 (2008). doi:10.1063/1.2897587
15. L. Assoufid *et al.*, *Rev. Sci. Instrum.* **87** (5), 052004 (2016). doi:10.1063/1.4950775
16. M. Sanchez Del Rio *et al.*, *J. Synchrotron Rad.* **27** (5), 1141 (2020). doi:10.1107/S1600577520009522
17. K. A. Goldberg *et al.*, *Opt. Lett.* **45** (17), 4694 (2020). doi:10.1364/OL.398737
18. K. A. Goldberg *et al.*, *Sensors* **21** (2), 536 (2021). doi:10.3390/s21020536
19. K. Desjardins *et al.*, IEEE Nuclear Science Symposium Conference Record, 2008, p. 2571. doi:10.1109/NSSMIC.2008.4774883
20. M. S. Rakitin *et al.*, *Proc. SPIE* **1149311**, 35 (2020). doi:10.1117/12.2569000